Optoelectronic property modeling of carbon nanotubes grafted with gold nanoparticles

2008 Nanotechnology 19 245702

(http://iopscience.iop.org/0957-4484/19/24/245702)

Nanotechnology **19** (2008) 245702 (8pp) doi:10.1088/0957-4484/19/24/245702

Optoelectronic property modeling of carbon nanotubes grafted with gold nanoparticles

Alex J Heltzel[1], Liangti Qu[2] and Liming Dai[2]

[1] P C Krause and Associates, Incorporated, West Lafayette, IN 47906, USA
[2] The University of Dayton Research Institute, Dayton, OH 45469, USA

Received 28 January 2008, in final form 3 April 2008
Published 12 May 2008
Online at stacks.iop.org/Nano/19/245702

Abstract
A three-dimensional (3D) electrodynamic model is built using the finite-difference time-domain (FDTD) method to investigate the optical response of carbon nanotubes grafted with gold nanoparticles. Theoretical characterizations suggest an anisotropic response, in line with previously observed absorption peaks of such systems in the optical range. An investigation of geometric and wavelength dependences is conducted, predicting the ability to tune the sub-wavelength intensity enhancement for efficient localization and propagation. The support of electric field enhancement along the nanotube walls raises the possibility of utilizing such systems as plasmon generators and waveguides for optical signal propagation.

Nomenclature

A_P	CP model amplitude parameter
E	electric field vector
G_P	critical points (CP) term
H	magnetic field vector
ε	electrical permittivity
ε_∞	relative permittivity at infinite frequency
γ	Drude contribution damping term
ϕ	phase
ω_D	plasma frequency
Γ_P	CP model broadening parameter
$\vec{\Psi}$	recursive accumulator
Ω_P	CP model gap energy parameter

1. Introduction

A wide, multidisciplinary field of study revolves around the geometric, power, and thermal challenges associated with shrinking semiconductor-based circuits. Well-known problems include thermal failure due to high density waste energy generation, and a dimensional limit for current lithographic techniques. Several problems can be alleviated or solved outright through the use of photonic devices as interconnects, though the wave properties of light constrain the miniaturization of light-based circuits. Photonic circuits, employed widely as fiber optic cables, have approximately three orders of magnitude greater data carriage capacity than electronic circuits. Diffraction limits their lower dimension to the order of a micrometer, making a coupling of optical fibers and electronic circuits in a microprocessor unfeasible. New concepts have been investigated, focusing on the interaction of light with noble metal nanoparticles [1]. Within such particles visible light can resonantly excite collective electron oscillations, known as surface plasmons [2]. Surface plasmon (SP) resonances in metallic nanoparticles are of interest for a variety of applications due to the large electromagnetic field enhancement that occurs at the interface between the metal and dielectric materials as well as the sub-wavelength localization of these fields. The high electron mobility in noble metals makes them useful electrical conductors and also attractive candidates for plasmonic applications. Advances in fabrication techniques that allow metals to be structured and characterized on the nanometer scale have facilitated the interest and research. Surface plasmons provide the mechanism (in theory) by which to bridge that dimensional gap and couple photonic and electrical signal processing. As conductors, surface plasmon waveguides could accomplish both, and do so at the nanoscale, breaking the bottleneck of interconnect capacity and allowing an increase in microprocessor speed.

The recent progress in pursuit of this goal has been exciting as the fundamental behaviors and SP propagation and decay are being uncovered. Weeber *et al* observed light propagating tens of microns on a 2.5 μm wide gold waveguide

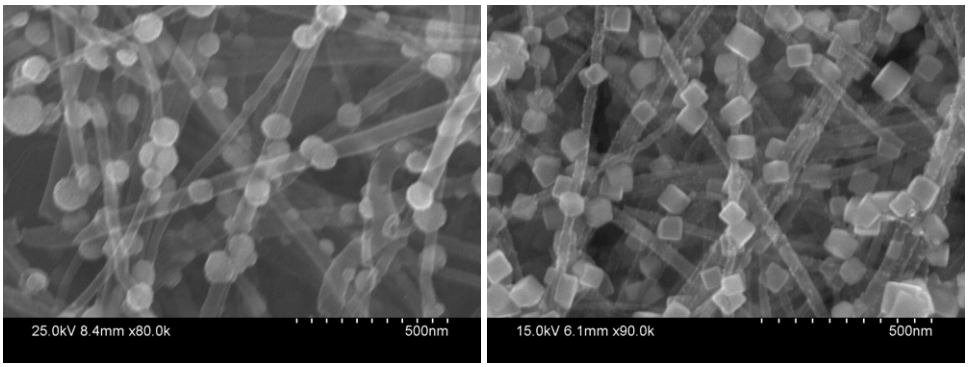

Figure 1. Typical SEM micrographs of a synthesized carbon nanotube grafted with gold nanosphere and nanocube systems.

before decay due to absorption and re-coupling to freely propagating radiation [3]. It has been shown that both silver and gold nanowires (20–100 nm diameter) can function as surface plasmon resonators, guiding an optical signal at least 10 μm in length [4, 5]. Semiconductor nanowires have also been used to guide light at sub-wavelength scales. Barrelet *et al* found that light can travel through sharp bends in cadmium sulfide nanowires with only moderate losses [6]. Greytak *et al* of the same research group used cadmium sulfide and gallium nitride nanowires as nanoscale lasers [7]. Sirbuly *et al* demonstrated coupling of GaN and ZnO nanowires with ribbon waveguides, and subsequent pulse lengths on the order of millimeters [8].

The integration of platinum and gold nanostructures with carbon nanotubes (CNTs) has been demonstrated recently, offering a unique capability to create periodic systems at a sub-wavelength scale [9]. In the study, a plasmonic absorption peak was observed, centered near $\lambda = 532$ nm wavelength. The work presented here gives the numerical solution to Maxwell's equations in the vicinity of such nanotube/nanostructure systems during irradiation by 355, 532, and 1064 nm light. The possibility of using such systems as photonic interconnects extends from other observations of anisotropic behavior in carbon nanotubes. Surface plasmons have been observed in multiwall CNTs using electron energy loss spectroscopy and fluorescent microbead detection [10–12].

There are two primary reasons for proposing carbon nanotubes as a potential plasmonic media. Theoretically, carbon nanotubes can be either semiconducting, semi-metallic, or metallic, depending on their chirality and thickness. Metallic CNTs have been shown to exhibit very small electrical resistance [13, 14]. This high conductivity should mitigate one of the largest factors in plasmonic decay: ohmic loss. More practically, mass fabrication (growth) of high quality carbon nanotubes has become possible and firmly established since the work of Ebbesen [15]. A computational investigation of plasmon generation and propagation in carbon nanotubes can therefore be a useful first step to introducing them as potential photonic interconnects.

2. Fabrication of CNT/gold nanostructures

The preparation process of gold nanoparticles grafted onto CNTs is similar to that in our previous report [9]. Briefly, in a typical experiment, CNT/gold nanospheres were produced by immersing Cu foil-supported CNTs into an aqueous solution of ~0.38 mM $HAuCl_4$ at room temperature for about 30 min, followed by thoroughly rinsing with distilled water. CNT/gold nanocubes were produced by immersing Cu foil-supported CNTs into an aqueous solution of ~1.9 mM $HAuCl_4$ with the addition of ~3 mM $CuCl_2$ at room temperature for about 10 s, followed by thorough rinsing with distilled water. Figure 1 shows typical scanning electron microscopy (SEM) images of a CNT modified with shape-controlled gold nanoparticles produced by the above procedure. As can be seen, Au nanospheres and nanocubes were multisite deposited along the nanotube length with individual nanotubes even threading through the nanoparticles. The size of the gold nanoparticles formed on CNTs in the above conditions is about 60–100 nm, while their size is feasibly tunable by controlling the deposition condition (e.g., reaction time) [9]. SEM imaging of the resultant samples was performed on a Hitachi S-4800 high resolution scanning electron microscope. UV–vis spectra were recorded on a Lambda 900 UV/VIS/NIR spectrometer (PerkinElmer).

The UV–vis absorption spectra for CNT/Au nanocube and CNT/Au nanosphere structures show similar surface plasmon resonances at about 530 nm (figure 2). Due to the absence of UV absorption above 400 nm for the pristine CNTs [9], the corresponding absorption peaks seen in the visible region for the CNT/nanoparticles arise mainly from the nanotube-supported Au nanoparticles.

3. Electrodynamic modeling

To predict the optical response of the nanotubes/nanostructure system, a 3D computational electrodynamics program was built based on the finite-difference time-domain (FDTD) method. The recursive convolution (RC) method was used in order to employ the critical points (CP) model recently presented for accurate treatment of gold in the optical range [16, 17]. In this model, the frequency-dependent optical properties can be represented by the infinite frequency response, ε_∞, a Drude contribution with plasma frequency, ω_D, and damping term, γ, along with two critical points terms representing the interband transitions in the violet/near-UV

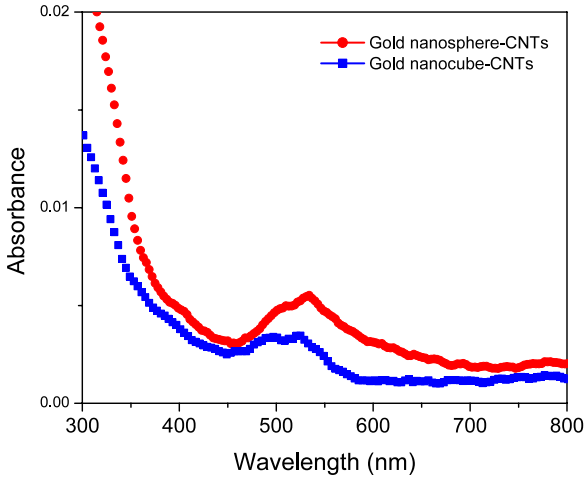

Figure 2. UV–vis spectra of CNTs grafted with gold nanospheres and nanocube particles dispersed in water by ultrasonication. (This figure is in colour only in the electronic version)

regions:

$$\varepsilon_{\mathrm{DCP}}(\omega) = \varepsilon_\infty - \frac{\omega_\mathrm{D}^2}{\omega^2 + \mathrm{i}\gamma\omega} + \sum_{P=1}^{2} G_P(\omega) \tag{1}$$

with

$$G_P(\omega) = A_P \Omega_P \left(\frac{\mathrm{e}^{\mathrm{i}\phi\gamma}}{\Omega_P - \omega - \mathrm{i}\Gamma_P} + \frac{\mathrm{e}^{-\mathrm{i}\phi\gamma}}{\Omega_P + \omega + \mathrm{i}\Gamma_P} \right). \tag{2}$$

The adjustable parameters in equation (2) represent the amplitude, A_P, gap energy, Ω_P, phase, ϕ, and broadening, Γ_P. A complete list of values for gold, silver, aluminum, and chromium, is given by Vial and Laroche [17], where they demonstrated accurate responses between 200 and 1000 nm for gold, silver, and aluminum, and between 400 and 1000 nm for chromium.

Recursive accumulators are then calculated within metallic regions of the FDTD domain, and included in the electric field updates, as given in equation (3).

$$\vec{E}\,|^{n+1} = \frac{\varepsilon_\infty}{\varepsilon_\infty + \chi^0}\,\vec{E}\,|^n + \frac{\Delta t}{\Delta x \varepsilon_0(\varepsilon_\infty + \chi^0)}\,\vec{\nabla} \times \vec{H}\,|^{n+1/2} + \frac{1}{\varepsilon_\infty + \chi^0}\,\mathrm{Re}\left(\vec{\Psi}_\mathrm{D}\,|^n + \sum_{m=1}^{2} \vec{\Psi}_m\,|^n \right). \tag{3}$$

The update equations for the Drude accumulator and CP accumulators are

$$\vec{\Psi}_\mathrm{D}\,|^n = \mathrm{e}^{-\gamma\Delta t}\,\vec{\Psi}_\mathrm{D}\,|^{n-1} - \left(\frac{\omega_\mathrm{D}}{\gamma}\right)^2 \left(1 - \mathrm{e}^{-\gamma\Delta t}\right)^2 \vec{E}\,|^n \tag{4}$$

$$\vec{\Psi}_m\,|^n = \Delta\chi_m^0\,\vec{E}\,|^n + \mathrm{e}^{(-\Gamma_m + \mathrm{i}\Omega_m)\Delta t}\,\vec{\Psi}_m\,|^{n-1}. \tag{5}$$

The quantities χ^0 and $\Delta\chi_m^0$ are defined as

$$\chi^0 = \chi_\mathrm{D}^0 + \mathrm{Re}\left(\sum_{m=1}^{2} \chi_m^0 \right) \tag{6}$$

$$\Delta\chi_m^0 = -\mathrm{i}\frac{2A_m\Omega_m \mathrm{e}^{-\mathrm{i}\phi_m}}{\Gamma_m - \mathrm{i}\Omega_m} \left(1 - \mathrm{e}^{(-\Gamma_m + \mathrm{i}\Omega_m)\Delta t}\right)^2, \tag{7}$$

and finally

$$\chi_\mathrm{D}^0 = -\left(\frac{\omega_\mathrm{D}}{\gamma}\right)^2 \left(1 - \mathrm{e}^{-\gamma\Delta t}\right) + \frac{\omega_\mathrm{D}^2}{\gamma}\Delta t \tag{8}$$

$$\chi_m^0 = -\mathrm{i}\frac{2A_m\Omega_m \mathrm{e}^{-\mathrm{i}\phi_m}}{\Gamma_m - \mathrm{i}\Omega_m} \left(1 - \mathrm{e}^{(-\Gamma_m + \mathrm{i}\Omega_m)\Delta t}\right). \tag{9}$$

This FDTD implementation therefore requires the additional vector fields $\vec{\Psi}_\mathrm{D}$, $\vec{\Psi}_1$, and $\vec{\Psi}_2$ in metallic regions, along with vector fields $\vec{E}$ and $\vec{H}$ in the whole domain. The drawback of increased storage can be mitigated by allocating memory only in the required metallic regions. Depending on the relative volumes of metal and dielectric/vacuum, the RC-FDTD implementation may then require less memory or substantially more memory than a typical ADE-FDTD method employing vector fields $\vec{E}$, $\vec{H}$, and current density $\vec{J}$ throughout the whole simulation domain.

Given the many variations in carbon nanotube chirality, inside diameter, outside diameter and number of wall layers, all of which affect the optical and electronic properties, certain generic assumptions must be made in order to model the interaction between light and a nanotube. First, the walls of a single wall nanotube consist of only one atomic layer. This structure can only be modeled with precision using molecular dynamics simulations, preferably quantum-based, and using *ab initio* derived data. Therefore, the decision was made to model multiwall tubes, where the optical response of ten to twenty atomic layers can be considered more homogeneous and fit within the context of the FDTD method and a dielectric function. The CNTs modeled here have inside diameters of 20 nm, and outside diameters of 40 nm, consistent with the experiments. Second, the nanotube's chirality is addressed only through the assumption of a metallic nanotube.

The optical response of nanotube arrays embedded in dielectric material has been fit successfully from the far infrared to the ultraviolet using a combined Drude–Lorentz model [11, 18].

$$\varepsilon(\omega) = \varepsilon_\infty - \frac{\omega_P^2}{\omega^2 - \mathrm{j}\,\omega\gamma_P} + \sum_j \frac{\omega_{P,j}^2}{\left(\omega_j^2 - \omega^2\right) - \mathrm{j}\Gamma_j\omega}. \tag{10}$$

The middle (Drude) term describes the metallic contribution of the tubes, and the third (Lorentz term) quantifies the response of the dielectric material. The dynamic response of the combined medium was then described in the referenced works by the Maxwell–Garnett model, which uses filling and geometric factors to determine the effective complex permittivity. Since we are not concerned with the dielectric medium, multiwall CNTs are modeled here by merely extracting the Drude values which fit the experimental data obtained from the research referenced above for use in the Drude term of equation (1). In particular, $\omega_P = 2.0$ eV and $\gamma_P = 0.2$ eV from Bommeli *et al* [11], and the infinite frequency response value of $\varepsilon_\infty = 3.49$ was used based on the work of Jeon *et al* [18].

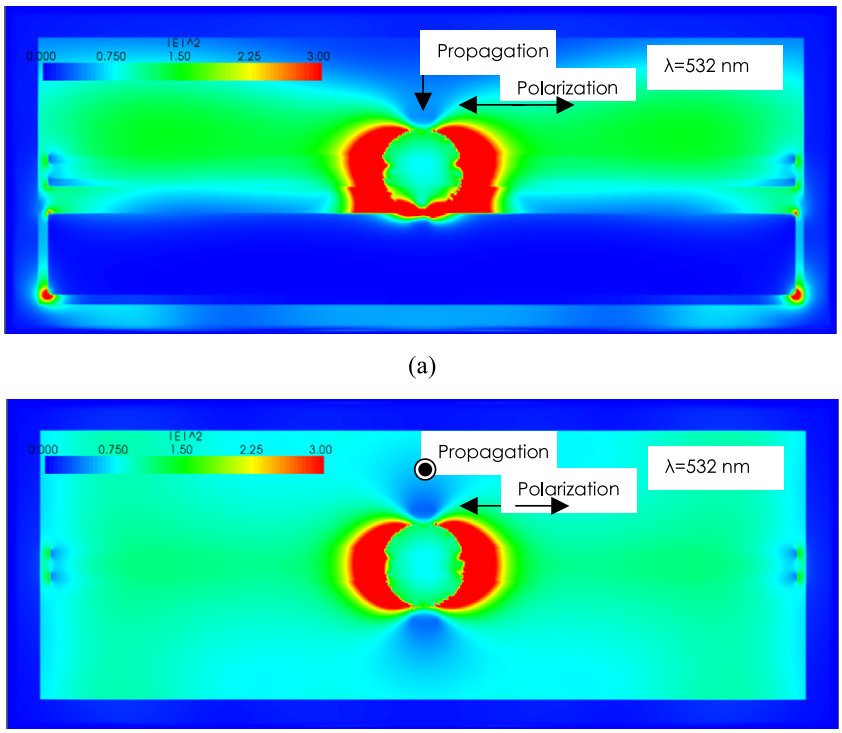

Figure 3. Electric field distribution surrounding an Au sphere-grafted carbon nanotube, $\lambda = 532$ nm, $\Delta = 2.0$ nm, (a) vertical plane, and (b) horizontal plane through CNT axis. Polarization parallel to the CNT axis.

The complex permittivity defined by these values is intended to represent an approximate cross section of metallic nanotubes, which are famously unique even within a common batch. A single Drude accumulator is then used in CNT domains in the FDTD update.

The details of the FDTD algorithm are covered in depth elsewhere [19] and therefore will not be addressed in this paper. The code was verified successfully against the analytical solution for a radiating dipole and comparison to Mie scattering theory. The convolutional perfectly matched layer (CPML) [20] was employed as an absorbing boundary condition, and the total field/scattered field construct [21] was used to generate the plane wave of the incident laser. Matched numerical dispersion was included to eliminate diffusive numerical error in long duration (time step) runs. The simulations presented here contain $200 \times 200 \times 500$ discrete Yee cells. Grid resolution was 2.0 nm, and converged fields were obtained after approximately 12 000 time steps.

4. Results and discussion

The initial modeling environment consists of a 100 nm diameter gold sphere embedded in a 900 nm segment of 40 nm outside diameter, 20 nm inside diameter carbon nanotube, positioned on a gold substrate, and irradiated by $\lambda = 532$ nm light normal to the substrate (second harmonic frequency of Nd:YAG laser). The light is polarized parallel to the substrate, parallel to the CNT axis, and perpendicular to its direction of propagation. Figure 3(a) presents the converged intensity distribution in the vertical mid-plane intersecting sphere, CNT, and substrate, with a spatial resolution of $\Delta = 2.0$ nm. Figure 3(b) gives the same quantity in the horizontal plane that passes through the CNT and sphere. In all simulations, the property of intensity refers to the time-averaged square of the electric field magnitude. The electric field plots are scaled between zero (dark blue) and three (red) times the magnitude of the incident pulse. Figure 4 presents the converged field for an identical simulation, with polarization still parallel to the substrate, but now perpendicular to the CNT axis.

The field shown in figures 3 and 4 indicates an enhancement of the light intensity in the near-field of the systems. Specifically, the surface of the gold nanospheres along the polarization axis, and near the gold substrate, exhibits a strong localized energy distribution. Another indication from figures 3 and 4 is the suggestion of Faraday shielding within the interior of the spheres and nanotubes. In this work, the CNTs are modeled as continuous through the Au spheres. The figures represent 2D slices midway through a 3D grid, so any interior field would be visible. The charge distribution near the metal surface, illustrated by the electric field enhancement, is characteristic of surface plasmon excitation at the gold sphere surface. The enhancement does not noticeably extend along the surface of the tubes, indicating a less-than-ideal situation for using the grafted sphere and CNT as a plasmon generator and waveguide system. Past work has demonstrated the utility of twin nanotube arrays, however, to guide electromagnetic energy [22]. Presumably, the negligible resistance in the volume between the CNTs allows propagation

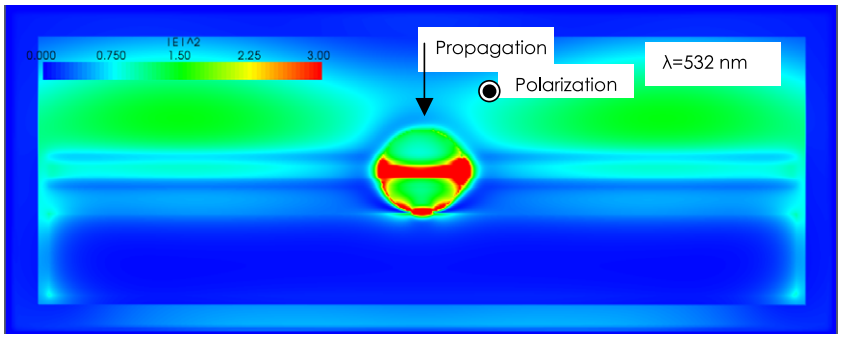

(a)

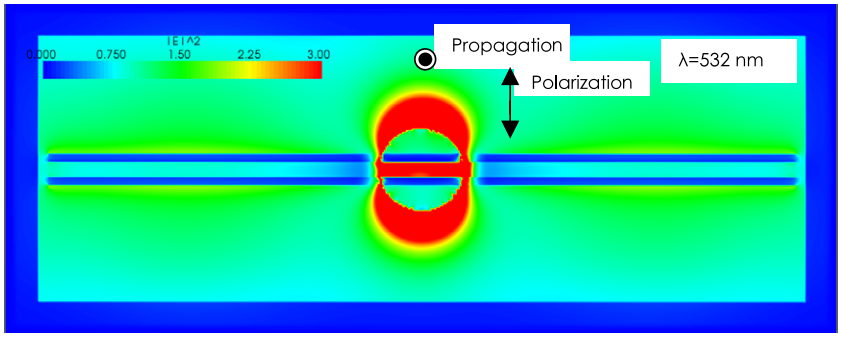

(b)

Figure 4. Electric field distribution surrounding an Au sphere-grafted carbon nanotube, $\lambda = 532$ nm, $\Delta = 2.0$ nm, (a) vertical plane, and (b) horizontal plane through CNT axis. Polarization perpendicular to the CNT axis.

of the surface wave, while the coupling of the surface energies on either tube keeps them localized to that low resistance volume. To investigate these phenomena, similar simulations were performed, replacing the single CNT with two CNTs of equal size, spaced 20 nm apart.

Figures 5 and 6 present the electric and magnetic field distributions, respectively, for the case of a 100 nm sphere grafted to twin nanotubes and irradiated with $\lambda = 532$ nm light, normal to the gold substrate. The light is polarized perpendicular to the CNT axes. In all other respects, the simulations in figures 5 and 6 are identical.

Figure 5 indicates the surface plasmon excitation along the surface of the nanotubes with intensity up to three times that of the incident field. The energy is enhanced and localized well below the diffraction limit; therefore the system can function as a sub-wavelength plasmonic waveguide. The coupled surface wave is generated after bridging the momentum gap using light/nanostructure interaction [23]. Comparing figures 3(a) and 5(a) indicates a re-distribution of charge in the vicinity of the sphere as well, possibly a result of coupling between the sphere and tube surface waves. The effect of polarization direction is significant, with no plasmon generation predicted along tube surfaces if the polarization is parallel to the tube axis (not shown).

The magnetic field distribution in figure 6 further reveals the nature of the enhancement. Whereas the electric field is stronger in the space between CNTs, peak magnetic field strength is localized in the volume between the CNT and the substrate. Likewise, the electric and magnetic field patterns surrounding the Au sphere are orthogonal, as may be expected.

The dependence of plasmon excitation on incident wavelength is also modeled here. Pulses of incident light with wavelengths $\lambda = 355$ and 1064 nm are modeled, in addition to $\lambda = 532$ nm above, corresponding to the fundamental, second harmonic, and third harmonic frequencies of an Nd:YAG laser. A more detailed investigation of frequency response could be performed by utilizing broadband pulses, but will remain a topic of future work. Figures 7 and 8 provide the electric field distribution in the vertical mid-plane for pulses of $\lambda = 355$ nm and $\lambda = 1064$ nm, respectively, with all other parameters identical to the $\lambda = 532$ nm simulation presented in figure 5. The plotting scale remains constant for comparison.

The response of the combined gold/CNT system reveals the independent dispersion properties of the two materials. While the 355 nm pulse excites plasmons of slightly higher intensity between the nanotubes, the gold sphere does not exhibit the strong local enhancement characteristic of the 532 nm pulse. Radiation of wavelength 1064 nm does not generate localized field magnitudes stronger than incident near either the gold sphere or CNTs. This behavior is consistent with the absorption spectra observed in figure 2, and the conclusion that absorption peaks seen in the visible region for the CNT/nanoparticles arise mainly from the Au nanoparticles. Quantitatively, the peak levels of enhancement at the three wavelengths are compared in figure 9. Previous work has shown that directing a component of polarization toward the substrate can cause extreme levels of localized intensity up to and exceeding 10^3 times incident. Such high levels of near-field enhancement have been utilized for

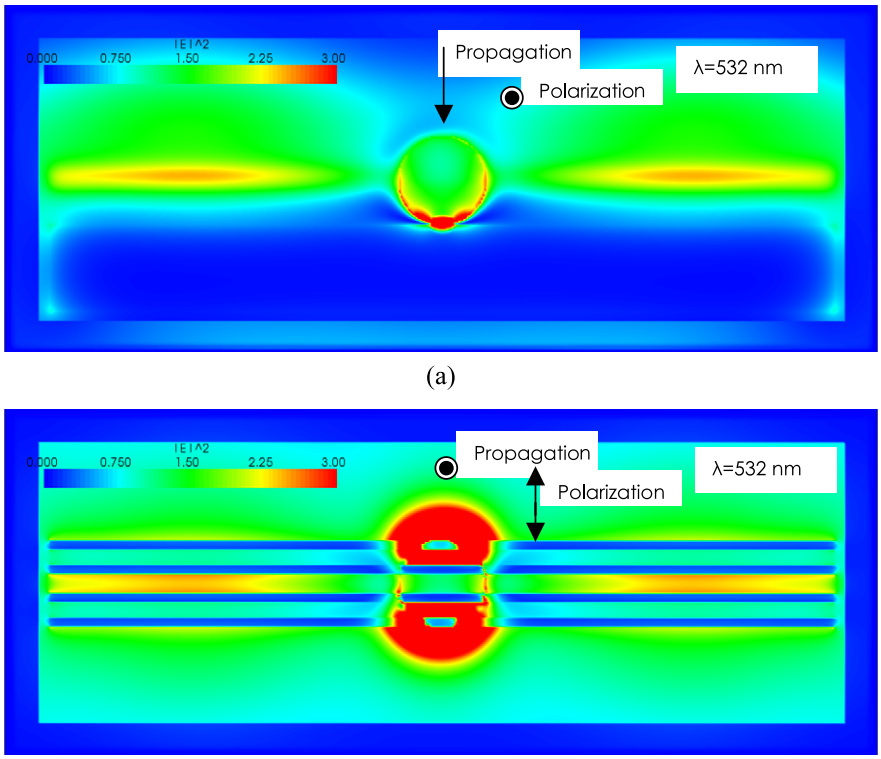

Figure 5. Electric field distribution surrounding Au sphere-grafted twin carbon nanotubes, $\lambda = 532$ nm, $\Delta = 2.0$ nm, (a) vertical plane, and (b) horizontal plane through the CNT axis. Polarization perpendicular to the CNT axis.

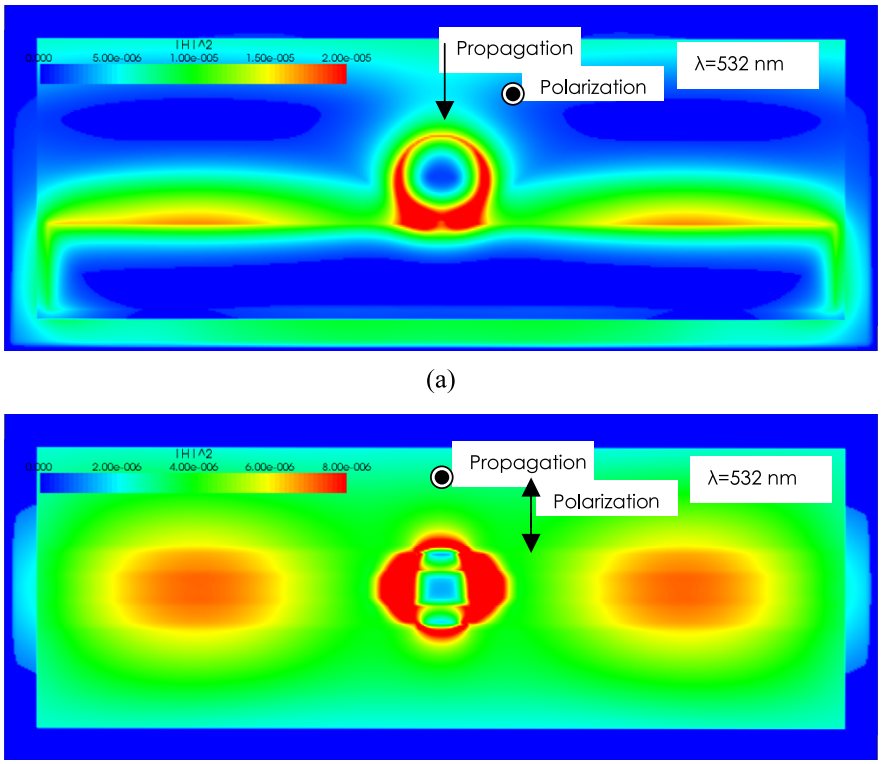

Figure 6. Magnetic field distribution surrounding Au sphere-grafted twin carbon nanotubes, $\lambda = 532$ nm, $\Delta = 2.0$ nm, (a) vertical plane, and (b) horizontal plane through the CNT axis. Polarization perpendicular to the CNT axis.

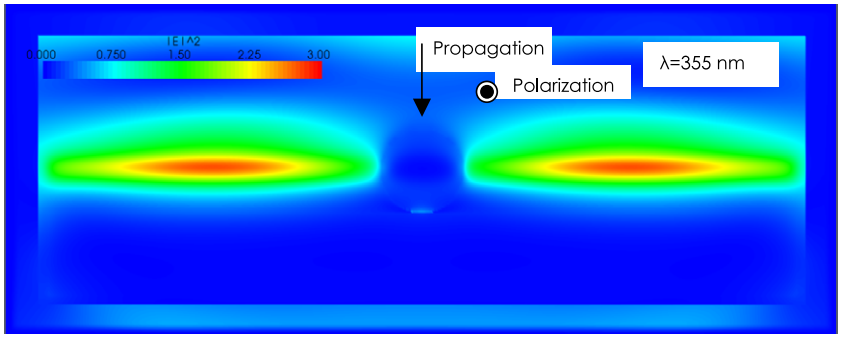

Figure 7. Electric field distribution surrounding Au sphere-grafted twin carbon nanotubes, $\lambda = 355$ nm, $\Delta = 2.0$ nm, (a) vertical plane, and (b) horizontal plane through the CNT axis. Polarization perpendicular to the CNT axis.

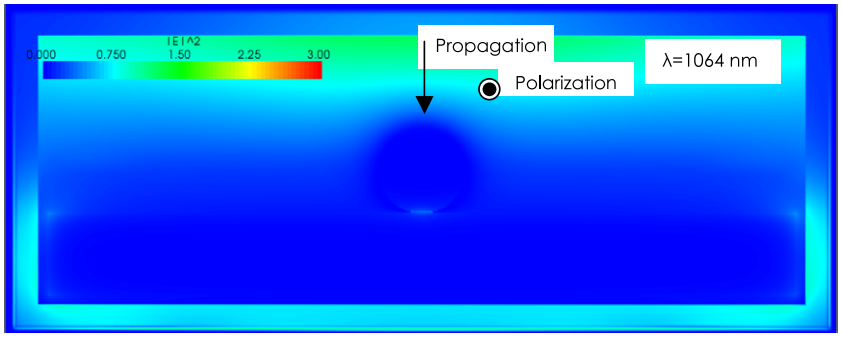

Figure 8. Electric field distribution surrounding Au sphere-grafted twin carbon nanotubes, $\lambda = 1064$ nm, $\Delta = 2.0$ nm, (a) vertical plane, and (b) horizontal plane through the CNT axis. Polarization perpendicular to the CNT axis.

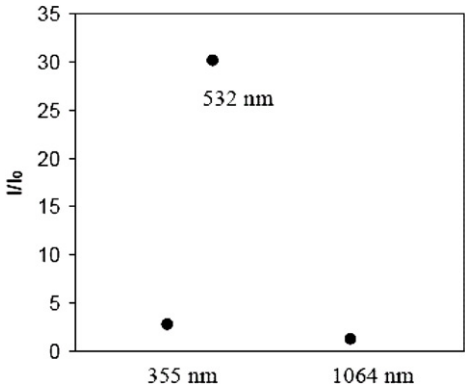

Figure 9. Peak enhancement values (normalized to incident) in a CNT/Au sphere system at three wavelengths.

lithographic purposes [24, 25]. An array of grafted CNTs could then provide the means to create repeatable sub-wavelength substrate patterning using a single optical pulse.

5. Conclusions

The ability to synthesize systems of carbon nanotubes conjoined with shape, size, and site selective metallic nanostructures has been demonstrated. Anomalous absorption has been observed consistent with the presence of surface plasmons. Light interaction with conjoined CNT/nanostructure systems has been modeled using the recursive convolution FDTD technique and the critical points model. The solutions to Maxwell's equations predict surface plasmon generation and guidance well below the diffraction limit. Plasmonic behavior is determined to be dependent on the spacing between nanostructures as well as the incident frequency. Based on the modeling presented here and recent observations, it can be concluded that metallic carbon nanotubes are a potential plasmonic waveguide medium and a step toward the goal of sub-wavelength photonic circuits.

References

[1] Klar T A, Perner M, Grosse S, Plessen G, Spirkl W and Feldmann J 1998 Surface-plasmon resonances in single metallic particles *Phys. Rev. Lett.* **80** 4249–52
[2] Raether H 1988 *Surface Plasmons* (Berlin: Springer)
[3] Weeber J C, Bourillot E, Dereux A, Goudonnet J-P, Chen Y and Girard C 1996 Observation of light confinement effects with a near-field optical microscope *Phys. Rev. Lett.* **77** 5332–5
[4] Ditlbacher H, Hohenau A, Wagner D, Kreibig U, Rogers M, Hofer F, Aussenegg F R and Krenn J R 2005 Silver nanowires as surface plasmon resonators *Phys. Rev. Lett.* **95** 257403
[5] Dickson R M and Lyon L A 2000 Unidirectional plasmon propagation in metallic nanowires *J. Phys. Chem.* B **104** 6095–8
[6] Barrelet C J, Greytak A B and Lieber C M 2004 Nanowire photonic circuit elements *Nano Lett.* **4** 1981–5
[7] Greytak A B, Barrelet C J, Li Y and Lieber C M 2005 Semiconductor nanowire laser and nanowire waveguide electro-optic modulators *Appl. Phys. Lett.* **87** 151103

[8] Sirbuly D J, Law M, Pauzauskie P, Yan H, Maslov A V, Knutsen K, Ning C-Z, Saykally R J and Yang P 2005 Optical routing and sensing with nanowire assemblies *Proc. Natl Acad. Sci.* **102** 7800–5

[9] Qu L, Dai L and Osawa E 2006 Shape/size-controlled synthesis of metal nanoparticles of site-selective modifications of carbon nanotubes *J. Am. Chem. Soc.* **128** 5523–32

[10] Bursill L A, Stadelmann P A, Peng J L and Prawer S 1994 Surface plasmon observed for carbon nanotubes *Phys. Rev.* B **49** 2882–7

[11] Bommeli F, Degiorgi L, Wachter P, Bacsa W S, de Heer W A and Forro L 1996 Evidence of anisotropic metallic behaviour in the optical properties of carbon nanotubes *Solid State Commun.* **99** 513–7

[12] Lu Q, Rao R, Sadanadan B, Que W, Rao A M and Ke P C 2005 Coupling of photon energy via a multiwalled carbon nanotube array *Appl. Phys. Lett.* **87** 173102

[13] Ebbesen T W, Lezec H J, Hiura H, Bennett J W, Ghaemi H F and Thio T 1996 Electrical conductivity of individual carbon nanotubes *Nature* **382** 54–6

[14] Gao B, Chen Y F, Fuhrer M S, Glattli D C and Bachtold A 2005 Four-point resistance of individual single-wall carbon nanotubes *Phys. Rev. Lett.* **95** 196802

[15] Ebbesen T W and Ajayan P M 1992 Large scale synthesis of carbon nanotubes *Nature* **358** 220–2

[16] Etchegoin P G, Le Ru E C and Meyer M 2006 An analytic model for the optical properties of gold *J. Chem. Phys.* **125** 167405

[17] Vial A and Laroche T 2007 Description of dispersion properties of metals by means of the critical points model and application to the study of resonant structures using the FDTD method *J. Phys. D: Appl. Phys.* **40** 7152–7158

[18] Jeon T-I, Kim K-J, Kang C, Mang I H, Son J-H, An K Y, Lee J Y and Lee Y H 2004 Optical and electrical properties of preferentially anisotropic single-walled carbon-nanotube films in terahertz region *J. Appl. Phys.* **95** 5736–40

[19] Taflove A and Hagness S 2005 *Computational Electrodynamics* 3rd edn (Boston, MA: Artech House)

[20] Gedney S D 1996 An anisotropic pml absorbing media for FDTD simulation of fields in lossy dispersive media *Electromagnetics* **16** 399–415

[21] Yee K S 1966 Numerical solution of initial boundary value problems involving Maxwell's equations in isotropic media *IEEE Trans. Antennas Propag.* **14** 302–7

[22] Heltzel A 2006 *PhD Dissertation* The University of Texas at Austin

[23] Barnes W L, Dereux A and Ebbesen T W 2003 Surface plasmon subwavelength optics *Nature* **424** 824–30

[24] Heltzel A, Theppakuttai S, Howell J R and Chen S C 2005 Analytical and experimental investigation of laser–microsphere interaction for nanoscale surface modification *J. Heat Transf.* **127** 1231–5

[25] Battula A, Theppakuttai S and Chen S 2006 Direct parallel nano-patterning of SiC by laser nanosphere lithography *J. Microlith. Microfab. Microsyst.* **5** 011009